Available online at www.sciencedirect.com
ScienceDirect
Earth and Planetary Science Letters 249 (2006) 173–187
EPSL
www.elsevier.com/locate/epsl

Polyphase inclusions in garnet–orthopyroxenite (Dabie Shan, China) as monitors for metasomatism and fluid-related trace element transfer in subduction zone peridotite

Nadia Malaspina [a,*], Jörg Hermann [b], Marco Scambelluri [a], Roberto Compagnoni [c]

[a] *Dipartimento per lo Studio del Territorio e delle sue Risorse, corso Europa, 26, 16132, Genova, Italy*
[b] *Research School of Earth Sciences, Australian National University, Mills Road, 0200, Canberra ACT, Australia*
[c] *Dipartimento di Scienze Mineralogiche e Petrologiche, via Valperga Caluso, 35, 10125, Torino, Italy*

Received 21 January 2006; received in revised form 10 July 2006; accepted 12 July 2006
Available online 17 August 2006
Editor: R.W. Carlson

Abstract

The ultrahigh-pressure (UHP) Maowu Ultramafic Complex (Dabie Shan, China) is hosted by coesite-bearing gneisses. Textural and geochemical data demonstrate that garnet–orthopyroxenites within the ultramafic complex derive from garnet–harzburgite precursors that have been metasomatised at peak UHP conditions (4.0±1.0 GPa, 750±50 °C) by the addition of a silica- and incompatible trace element-rich fluid phase (hydrous melt), sourced from the associated crustal rocks. This metasomatism produced poikilitic orthopyroxene with high LREE and Ni contents and inclusion-rich garnet porphyroblasts. Solid polyphase primary inclusions within peak metamorphic garnet display negative crystal shapes and constant volume ratios of infilling mineral phases. Experimental homogenisation of these inclusions at conditions close to the estimated metamorphic peak demonstrates that the polyphase inclusions derive from trapped solute-rich aqueous fluids. The trace element characteristics of the experimentally re-homogenised inclusions include high LREE contents, a pronounced enrichment in LILE, with spikes of Cs, Ba, Pb and high U/Th.

The investigated UHP garnet–orthopyroxenites from Maowu represent a natural laboratory to constrain the trace element transfer from the subducted crust to the mantle wedge at sub-arc depths. The observed textures and chemical characteristics provide evidence for the infiltration of a felsic hydrous melt into garnet–peridotite, a circumstance comparable to expected interaction of sediment-derived melts with mantle wedge peridotites in subduction zones. The SiO_2 and Al_2O_3 component of the hydrous melt reacted with olivine to form replacive orthopyroxene and new garnet. The neoblastic orthopyroxene is able to accommodate some of the LREE, whereas the H_2O and LILE component of the melt were partitioned into a residual aqueous fluid phase. Remnants of such an aqueous fluid were trapped in the garnet and formed the polyphase inclusions. The trace element pattern of these inclusions is very similar to the incompatible element enrichment observed in arc lavas. We suggest that the residual fluid produced by the peridotite/hydrous melt reaction is able to transfer the characteristic LILE signature from the subducted sediments to the locus of partial melting in the mantle wedge. Moreover, this study provides evidence that polyphase inclusions are important tools for constraining the nature and composition of UHP fluids.

Keywords: polyphase inclusions; orthopyroxenite; mantle wedge; trace element transfer; UHP metasomatism; subduction

* Corresponding author. Tel.: +39 010 353 8137; fax: +39 010 352169.
E-mail address: malaspina@dipteris.unige.it (N. Malaspina).

0012-821X/$ - see front matter © 2006 Elsevier B.V. All rights reserved.
doi:10.1016/j.epsl.2006.07.017

1. Introduction

Fluids released by subducting plates recycle incompatible elements in the Earth's mantle and trigger metasomatism and partial melting in the supra-subduction zone mantle wedge [1–4]. The composition of such fluids is still a matter of debate [5–7]. It also remains unresolved whether the fluid phase corresponds to an aqueous solution, a hydrous silicate melt, or to a solute-rich supercritical fluid, which is intermediate between these two end members [3,8–12]. Despite significant advancements in the understanding of slab fluids, knowledge about their interaction with the mantle wedge is still scarce. This represents a key evolutionary step in the overall element recycling process, which is mostly approached by means of laboratory experiments and geochemical modelling [13]. A full understanding of these processes requires suitable rock samples that enable detailed investigation of the interactions between mantle peridotite and incoming subduction fluids at sub-arc depths. Most studies of supra-subduction zone peridotites investigated either fore-arc peridotite xenoliths, or xenoliths sampled at relatively shallow mantle levels, well above arc-magma sources [14–16]. Alternatively, information on deep metasomatism of the mantle wedge can be gained by the study of ultrahigh-pressure (UHP) terrains that contain felsic rocks and metasomatised peridotites [17–19]. Such associations represent unique natural laboratories to study element exchange between crustal and mantle rocks at pressures corresponding to the sub-arc depth of the subducted slab [12]. In these terrains, remnants of the fluid phase present at UHP may be preserved as primary polyphase inclusions in UHP minerals. These inclusions show the same textural features as fluid inclusions and locally may enclose UHP minerals such as diamond [20–22]. The discovery of such polyphase inclusions in UHP minerals (e.g. garnet) [20,23], opened new perspectives on the nature of UHP fluids. Detailed textural studies [23,24], as well as experimental attempts to homogenise such inclusions [25], demonstrate that polyphase inclusions derive from solute-rich aqueous fluids or hydrous melts. Such inclusions can be analysed by Laser-Ablation ICP-MS providing crucial information on the original trace element characteristics of the trapped fluid [22,26,27].

With this scenario in mind, we focussed on the Dabie-Sulu UHP complex, which represents the largest known slice of deeply subducted continental crust. We have investigated in detail garnet–pyroxenites cropping out in the Maowu Ultramafic Complex from Dabie Shan. This body consists of layered mafic/ultramafic rocks ranging from harzburgites to orthopyroxenites, which are associated with coesite eclogites and hosted by garnet–coesite-bearing gneisses [28–31]. In this terrane, gneisses and ultramafic rocks share a common metamorphic history [30–32], allowing investigation of element transfer in crust–mantle systems. Here we present a petrologic, geochemical and experimental study of garnet–orthopyroxenites and websterites that were derived from crustal metasomatism at UHP conditions. We describe in detail the textures and trace element compositions of polyphase inclusions that are hosted by peak metamorphic garnet and show that such inclusions represent a trapped solute-rich aqueous fluid. This study provides direct insights on fluid-mediated crust-to-mantle trace element transfer at sub-arc depths.

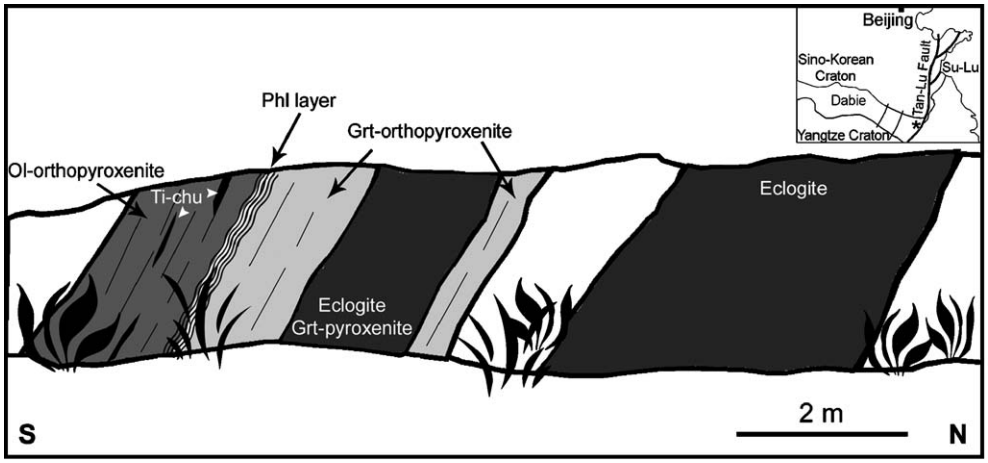

Fig. 1. Simplified cross section of the mafic/ultramafic outcrop at Maowu. Inset: geographic location of the Maowu complex in the Dabie belt, Eastern China.

2. Geological background and petrographic description

The Maowu Ultramafic Complex is a large E–W trending lenticular body hosted by gneissic rocks, located in the UHP metamorphic belt of the Dabie Mountains, China (Fig. 1). It consists of metre- to centimetre-thick layers of garnet–orthopyroxenites, clinopyroxenites, websterites, and harzburgites, associated with eclogites and coesite-bearing omphacitites. The boundaries between the different rock types are parallel to the main foliation of the host gneiss and locally develop mylonitic layers. The mafic/ultramafic body is in fault contact with country rocks, which mainly consist of biotite gneiss, marble, garnet-bearing gneiss and amphibolite [30,33]. Coesite inclusions in zircon [29] and quartz pseudomorphs after coesite in garnet [28,33] have been discovered in garnet–biotite-bearing gneisses. Also, garnet and pyroxene in marble contain quartz pseudomorphs after coesite and calcite pseudomorphs after aragonite [29,33], implying that the peak mineral assemblage formed under UHP conditions. Previous structural analyses and petrological studies suggested that the Maowu Ultramafic Complex, the coesite-bearing eclogite, marble and the host gneiss all experienced coeval UHP metamorphism during the Triassic collision between the Sino-Korean and Yangtze cratons [30,31,33]. On the basis of geochemical and isotopic data, the Maowu Complex has been interpreted as a layered intrusion composed of cumulate rocks (mainly orthopyroxenites), which underwent crustal contamination and post-magmatic metasomatism prior to the peak metamorphism [31,34,35]. The observed parageneses and the mineral compositions of harzburgites and garnet–pyroxenites indicate peak metamorphism at 4.0±1.0 GPa and 750±50 °C [31,35,36].

Selected samples of garnet–orthopyroxenites and websterites have been collected near the village of Shima. The outcrop consists of alternating eclogite and orthopyroxenite (Fig. 1) displaying a colour variation due to the different content of garnet, orthopyroxene, clinopyroxene and olivine. The boundaries between the different layers are sharp and parallel to the main

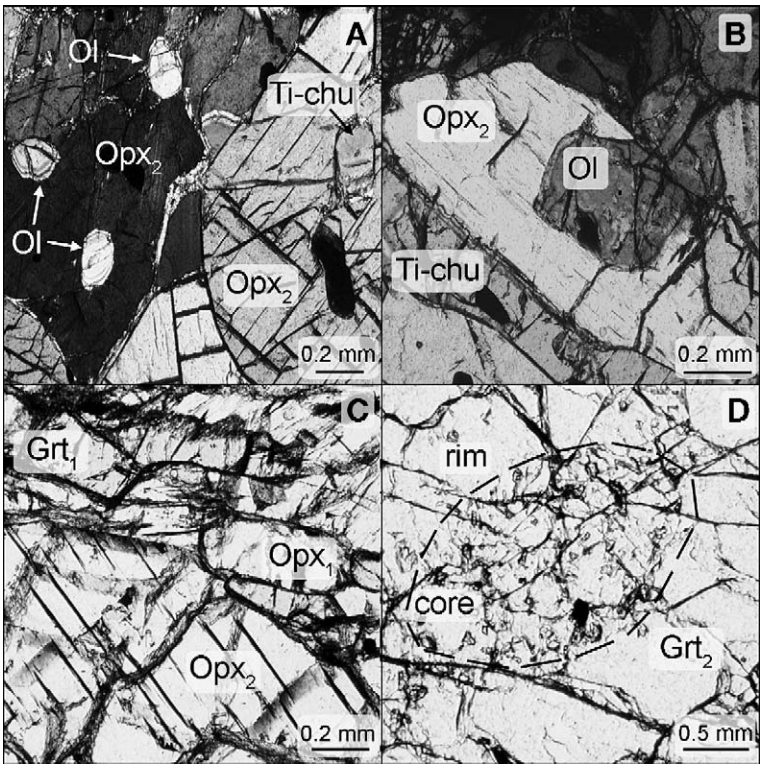

Fig. 2. Photomicrographs of representative rock-forming minerals in the Maowu orthopyroxenites. A: Transmitted light image (crossed polarised light) of coarse orthopyroxene (Opx_2) hosting corroded grains of olivine and Ti-clinohumite. B: Transmitted light image (crossed polarised light) of an olivine bleb partly overgrown by Opx_2. C: Transmitted light image (plane polarised light) of fine-grained orthopyroxene (Opx_1) associated with inclusion-free, fine-grained garnet (Grt_1). Note the textural difference between Opx_1 and the coarser Opx_2. D: Transmitted light image (plane polarised light) of coarse and zoned garnet (Grt_2), with inclusions-rich core and clear rim. Mineral abbreviations after Bucher and Frey [49].

foliation. Locally, phlogopite-rich horizons develop adjacent to the orthopyroxenite layers (Fig. 1). The studied pyroxenites display an assemblage dominated by orthopyroxene, garnet and minor clinopyroxene. Discontinuous layers of Ti-clinohumite and Ti-chondrodite are locally present. The samples are strongly foliated, with centimetre-thick layers of coarse, oriented orthopyroxene, and layers where orthopyroxene coexists with coarse zoned garnet. All samples show equilibrium texture among minerals with 120° triple junctions, but an older assemblage is still preserved. Such relict mineral association consists of olivine, orthopyroxene (Opx_1), garnet (Grt_1), and subordinated Ti-clinohumite and Ti-chondrodite. These minerals are diffusely overgrown by poikilitic orthopyroxene (Opx_2). Olivine occurs both as corroded grains and as isolated blebs within the coarse Opx_2 (Fig. 2A,B). Opx_2 also includes older fine-grained Opx_1, which is associated with the relict olivine and with fine-grained unzoned garnet (Grt_1) (Fig. 2C). Ti-clinohumite and Ti-chondrodite display the same textures as olivine (Fig. 2A), predating the Opx_2 stage formation. The observed petrographic texture documents the replacement of former SiO_2-undersaturated phases, such as olivine and Ti-clinohumite, by new orthopyroxene. The garnet-rich layers are composed of millimetre- to centimetre-sized garnet (Grt_2), which is texturally different from Grt_1. Zonation of Grt_2 is evident in thin section with cores appearing dusty due to disseminated polyphase microinclusions, whereas rim zones appear clear and inclusion-free (Fig. 2D).

Abundant polyphase solid inclusions occur as clusters within the core of porphyroblastic Grt_2 (Fig. 2D). These inclusions display regular negative-crystal shapes and constant volume proportions of the infilling phases. This suggests that the inclusions are primary and likely derive from a trapped fluid or melt. Petrographic observations (Fig. 3A,B), electron microscope imaging (Fig. 3C,D) and SEM analysis reveal that the inclusions consist of about 10–20 vol.% of spinel and of 80–90 vol.% of hydrous phases including amphibole + chlorite ± talc ± mica ± apatite. Sulfide was identified in rare cases.

3. Analytical and experimental techniques

3.1. Major and trace element analyses

Bulk-rock major and trace element concentrations, and mass loss on ignition, were determined on rock

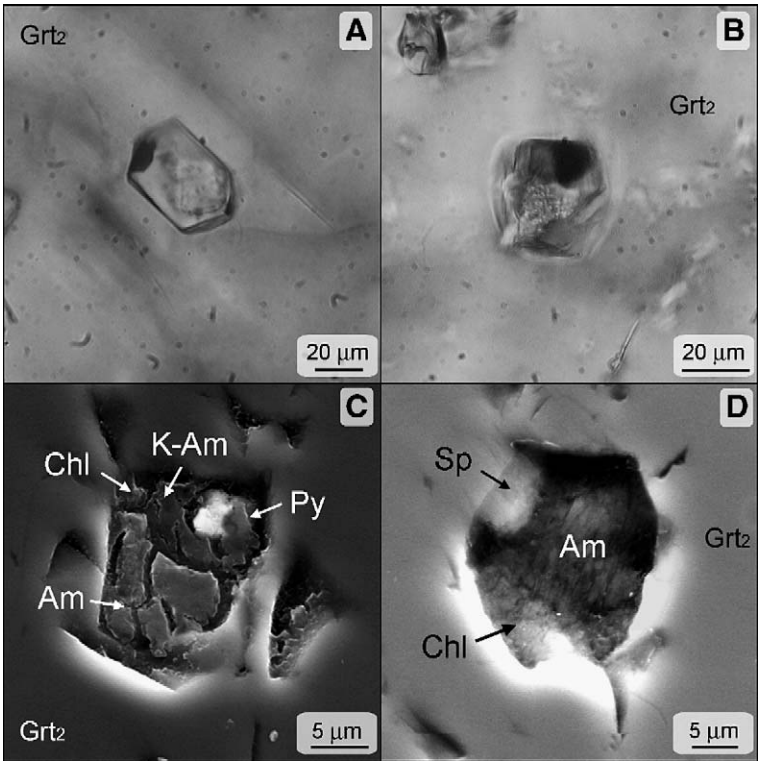

Fig. 3. Photomicrographs of polyphase solid inclusions in Grt_2 cores. A, B: Plane polarised transmitted light images; C, D: Secondary electron images. Mineral abbreviations after Bucher and Frey [49].

glasses by standard XRF and by Laser Ablation Inductively-Coupled Plasma Mass Spectrometry (LA ICP-MS), respectively, at the Activation Laboratories Ltd. (Ancaster, Ontario).

Major elements of rock-forming minerals were analysed by wavelength dispersive spectrometry using a Cameca SX 100 electron microprobe at the Research School of Earth Sciences (RSES), Australian National University (ANU). Acceleration voltage was set to 15 kV and beam current was 20 nA. Mineral analyses were always assisted by back-scattered electron (BSE) images to control the microtextural site. Trace element mineral compositions were acquired by LA ICP-MS at the RSES (ANU). The LA ICP-MS technique, employs an ArF (193 nm) EXCIMER coupled with an Agilent 7500 quadropole ICP-MS. Spot sizes of 187 and 112 μm were used for mineral phases and the counting time was 17 s for the background and 60 s for sample analyses. ^{43}Ca and ^{29}Si were employed as the internal standard isotope, based on CaO and SiO_2 concentrations previously measured by electron microprobe. NIST-612 and NIST-610 glasses were used as the external standards, assuming the composition given by Pearce et al. [37]. A BCR-2G glass was used as a secondary standard. Reproducibility about the mean values of 8 analyses were between 0.5 and 4% relative (1σ) for most of elements. The average of this glass yielded trace element contents that were typically within 2–6% of the certified values for this standard [38].

The mineral phases of polyphase and experimentally homogenised inclusions in garnet were qualitatively determined with a Philips SEM 515 electron microscope at the University of Genova. The accelerating potential was 15 kV, the beam current 20 nA, and the counting time 100 s. Natural minerals were used as standards. The trace element compositions of inclusions were acquired by LA ICP-MS at the RSES (ANU) at similar running conditions as those described above, but with a spot size of 112 μm. The SiO_2 wt.% of bulk solid inclusions has been estimated by calculating a weighted mean of the SiO_2 content of the infilling mineral phases. Since the resulting SiO_2, ranging from ~ 33 to ~ 40 wt.%, is comparable with the concentrations in the host garnet, ^{29}Si was used as internal standard based on SiO_2 concentrations measured in garnet. The single inclusion or cluster of inclusions occupies from 5 to 25 vol.% of the laser spot, whereas the host garnet comprises the remainder the analysis. The trace element compositions reported in Table 2 and the Primitive Mantle normalised patterns of Fig. 5, therefore, do not correspond to the absolute concentrations of inclusions. Such values have to be interpreted as the result of garnet + inclusion concentrations.

3.2. Piston cylinder experiments

The experimental inclusion re-homogenisation was performed in an end-loaded 1.27 cm piston-cylinder apparatus at the RSES, ANU. The garnets were then loaded as layers alternating with powdered garnet–orthopyroxenite sample into an Au capsule (outside diameter = 2.3 mm). 23 mg of $AlOH_3$ was added at the base of the charge, which produced about 8% of H_2O in the experiment. The water and rock powder were added to form a comparable environment outside and within the polyphase inclusions to minimise decrepitation during homogenisation procedures. Additionally this setup permits evaluation of whether or not the rock was above the wet solidus at run conditions. The capsule was sealed by arc welding while immersed in water-soaked tissue paper to prevent water loss. A low friction assembly was used consisting of teflon foil, NaCl and pyrex sleeves, a graphite heater and sintered MgO inserts, in which the Au capsule was embedded. The experiment was run at 3.5 GPa and 900 °C for 48 h. Pressure in the experiments was measured by load on the piston and is accurate to ± 0.1 GPa. Pressure was adjusted several times during the first 24 h of runs to compensate pressure drop due to the release of internal friction. Temperature, controlled by using type B thermocouples ($Pt_{94}Rh_6$/$Pt_{70}Rh_{30}$), was accurate to ± 10 °C. At the end of the run, the capsule was first pierced and the escape of an aqueous fluid was observed. Then the capsule was dried, opened and the separated garnets were extracted. Then the garnets were mounted in epoxy and the inclusions were exposed. The rock powder did not produce any glass in the capsule, indicating that the experimental conditions were below the wet solidus for the garnet–orthopyroxenite system.

4. Results

4.1. Whole-rock compositions

On the basis of textural relationships, we chose three representative samples of (i) orthopyroxenite with relict olivine, (ii) garnet-rich orthopyroxenite, and (iii) clinopyroxene-bearing orthopyroxenite (websterite) for detailed analyses. The whole-rock major and trace element compositions of the three selected samples are reported in Table 1. These orthopyroxenites are characterised by high Mg number (Mg# = 89–91), and high Ni contents. In a Mg# versus Ni diagram they plot very close to the Depleted Mantle [39], indicating that they derive from a peridotite protolith (Fig. 4A). In contrast, other pyroxenites and eclogites from Maowu, attributed to

recrystallisation of initial mafic cumulates [35] have lower Mg# and Ni contents, in agreement with the proposed cumulate origin. With respect to peridotite, the three studied samples have higher SiO_2 content, up to ~ 54 wt.%. Relatively low CaO contents (Table 1) suggest that the protolith was a harzburgite, rather than a

Table 1
Major (wt.% oxide) and trace (ppm) element compositions of whole-rocks and of representative rock-forming minerals

	ol-orthopyroxenite	grt-orthopyroxenite	websterite	Ol	Opx_1	Opx_2	Cpx	Grt_1	Grt_2
SiO_2	47.16	53.85	52.70	38.69	56.83	57.56	54.71	39.75	40.73
Al_2O_3	4.04	3.54	2.36	bdl	0.04	0.06	0.18	20.47	23.52
Fe (tot)	†8.10	†6.86	†7.93	‡7.27	‡4.29	‡4.31	‡1.39	‡14.30	‡11.72
MnO	0.12	0.11	0.12	0.02	0.11	0.07	0.05	0.45	0.58
MgO	37.11	33.74	32.97	53.13	38.43	38.70	18.39	23.15	21.84
CaO	0.29	0.36	2.70	0.01	0.05	0.03	24.58	2.29	1.47
Na_2O	bdl	0.02	0.32	bdl	bdl	bdl	0.27	bdl	bdl
K_2O	0.02	0.02	0.01	bdl	bdl	bdl	bdl	bdl	bdl
TiO_2	1.47	0.20	0.59	bdl	0.02	0.06	0.11	bdl	bdl
Cr_2O_3	0.24	0.27	n.a.	0.02	0.06	0.09	0.42	0.50	0.20
Total	100.30	100.10	99.75	99.13	99.85	100.88	100.10	100.91	100.06
Mg#	90	91	89	0.92	0.94	0.94			
LOI	1.67	1.10	0.37						
Li	n.a.	n.a.	n.a.	2.00	0.56	0.26	1.08	2.81	0.49
Be	n.a.	n.a.	n.a.	0.02	0.53	0.48	1.40	0.30	bdl
P	524	43.6	131	267	14.6	11.4	10.0	223	188
Sc	n.a.	n.a.	12.9	2.40	1.92	1.94	4.52	43.2	58.2
V	28.0	76.0	n.a.	2.83	5.11	5.07	68.1	62.3	73.7
Cr	1780	1640	1449	n.a.	n.a.	n.a.	n.a.	n.a.	n.a.
Ni	1430	2210	1406	7017	1257	2829	730	165	157
Cu	bdl	bdl	13.3	n.a.	n.a.	n.a.	n.a.	n.a.	n.a.
Zn	40.0	50.0	43.4	n.a.	n.a.	n.a.	n.a.	n.a.	n.a.
Ga	3.00	4.00	3.17	n.a.	n.a.	n.a.	n.a.	n.a.	n.a.
Ge	1.00	1.00	n.a.	n.a.	n.a.	n.a.	n.a.	n.a.	n.a.
Rb	bdl	bdl	0.15	bdl	bdl	bdl	0.08	0.18	bdl
Sr	4.00	22.0	23.6	0.02	0.10	0.77	263	1.16	0.04
Y	5.00	8.00	3.74	0.01	0.03	0.17	1.11	17.6	34.9
Zr	14.0	30.0	3.05	0.05	0.01	0.01	0.14	3.92	3.59
Nb	2.00	13.0	4.94	0.15	0.003	0.003	0.005	0.09	0.02
Cs	bdl	bdl	0.06	bdl	bdl	bdl	bdl	0.05	bdl
Ba	13.0	39.0	2.78	0.34	0.16	1.48	0.60	10.6	0.03
La	0.50	1.50	0.97	bdl	0.004	0.11	2.33	0.03	0.01
Ce	0.80	0.80	1.48	bdl	0.01	0.05	5.67	0.06	0.04
Pr	0.08	0.24	0.30	bdl	0.002	0.02	1.37	0.01	0.01
Nd	0.40	1.00	1.32	bdl	0.01	0.08	6.56	0.17	0.24
Sm	0.10	0.20	0.53	bdl	bdl	0.02	2.22	0.39	0.60
Eu	0.12	0.12	0.19	bdl	0.003	0.01	0.57	0.26	0.39
Gd	0.40	0.50	0.72	bdl	0.01	0.03	1.53	1.71	2.67
Tb	0.10	0.10	0.12	bdl	bdl	0.005	0.13	0.45	0.72
Dy	0.80	1.00	0.76	bdl	bdl	0.02	0.43	3.33	6.06
Ho	0.20	0.20	0.15	bdl	bdl	0.004	n.a.	0.65	1.38
Er	0.50	0.60	0.39	bdl	bdl	0.01	0.08	1.72	4.03
Tm	0.08	0.10	0.06	bdl	bdl	bdl	n.a.	0.23	0.59
Yb	0.50	0.70	0.35	bdl	bdl	bdl	0.04	1.49	3.89
Lu	0.06	0.11	0.06	bdl	bdl	bdl	0.004	0.21	0.57
Hf	0.40	0.80	0.09	bdl	bdl	bdl	bdl	0.06	0.05
Ta	0.20	0.90	0.37	bdl	bdl	bdl	bdl	bdl	bdl
Pb	bdl	bdl	4.45	bdl	0.10	0.34	1.63	0.16	0.19
Th	0.20	bdl	0.16	bdl	bdl	0.02	bdl	bdl	0.03
U	bdl	bdl	0.09	bdl	bdl	0.003	bdl	bdl	0.02

Mineral abbreviations from Bucher and Frey [49].
† = Total iron as Fe_2O_3; ‡ = Total iron as FeO; bdl = below detection limits; n.a. = not analysed.

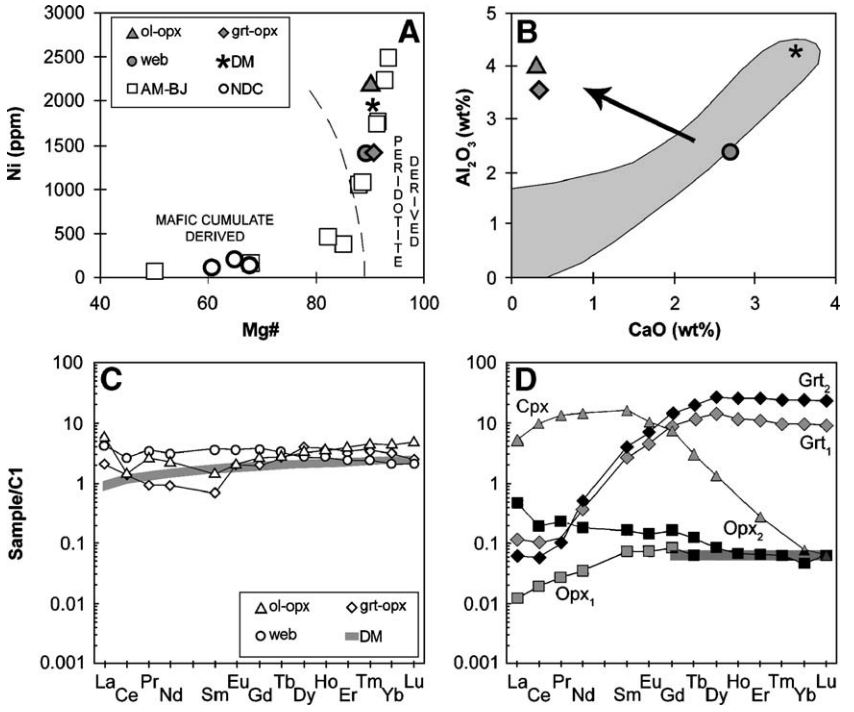

Fig. 4. A: Mg# versus Ni (in ppm) plot of orthopyroxenites (this work) and of harzburgites, garnet–orthopyroxenites, garnet–websterites, garnet–clinopyroxenites and eclogites from Maowu layered intrusion [35]. For comparison, Depleted Mantle [39] and mafic rocks data from the North Dabie Complex [50] are also reported. The shaded line represents the possible transition from cumulates to peridotites. B: CaO versus Al_2O_3 wt.% concentrations of the studied samples and of Depleted Mantle. The compositional variation of orogenic, ophiolitic and abyssal peridotites is also showed in the grey field (from Bodinier and Godard [40]). The black solid arrow represents the relative enrichment in Al_2O_3 with decreasing CaO of Maowu orthopyroxenites, compared with the grey area representing a peridotite depletion trend starting from the composition of Depleted Mantle [39]. C: Chondrite (C1) [51] normalised bulk-rock REE patterns are compared with Depleted Mantle (grey line) from Salters and Stracke [39]. D: Chondrite (C1) [51] normalised REE patterns of rock-forming minerals. Concentrations of each mineral phase are average of 5 representative analyses. The grey transparent line represents the detection limits for HREE. Mineral abbreviations after Bucher and Frey [49]; grt–opx = garnet-rich orthopyroxenite; web = websterite; ol–opx = orthopyroxenite with relict olivine; DM = Depleted Mantle; AM–BJ = mafic and ultramafic samples from Jahn et al. [35]; NDC = North Dabie Complex eclogites from Malaspina et al. [50].

lherzolite. However, the studied rocks have high Al_2O_3/CaO (10–14), as shown in Fig. 4B, where the black arrow indicates an increase of Al_2O_3 with decrease of CaO. This compositional variation contrasts with a peridotite depletion trend (grey field in Fig. 4B [40]), suggesting that the analysed Maowu orthopyroxenites are selectively enriched in Al_2O_3 with respect to CaO.

The trace elements whole-rock concentrations are reported in Table 1, and the Chondrite (C1) normalised Rare Earth Element (REE) are portrayed in Fig. 4C. Overall, the three samples show similar patterns, resembling the Depleted Mantle [39], particularly for the Medium (MREE) and Heavy REE (HREE). Light REE (LREE) of the orthopyroxenites are enriched with respect to the Depleted Mantle. On the other hand, the pyroxenites do not record a comparable enrichment in other incompatible elements, i.e. the Large Ion Lithophile Elements (LILE), which are mostly below the detection limits (Table 1).

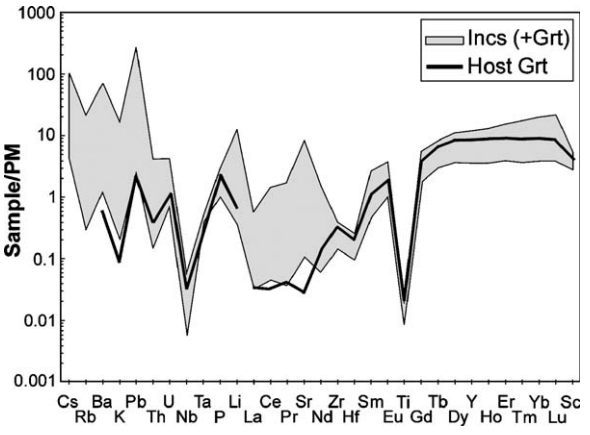

Fig. 5. Primitive Mantle (PM) [49] normalised trace element compositions of all the polyphase inclusions analysed (grey area), compared with an average pattern of inclusion-free domains in the host garnet. Abbreviations: Incs (+Grt) = bulk inclusions analyses resulting as mixture of polyphase inclusions and the host garnet.

4.2. Mineral compositions

Major and trace element mineral compositions are consistent with the ultramafic nature of the studied pyroxenites (Table 1). Olivine has 90 to 93 mol% of forsterite and shows high Ni contents. Both Opx_1 and Opx_2 have high Mg# (93–94), low CaO (0.03–0.09 wt.%) and low Al_2O_3 (<0.1 wt.%). Grt_1 and Grt_2 are both pyrope-rich (70–73%). Grt_2 shows a decrease in FeO_{tot} and MgO with respect the older Grt_1 (Table 1).

Chondrite-normalised REE patterns of average mineral concentrations are portrayed in Fig. 4D. Clinopyroxene is enriched in LREE and depleted in HREE, showing equilibrium partitioning with garnet. Grt_1 and Grt_2 share HREE-enriched patterns, with absolute concentrations up to 20–30 times chondritic values. Opx_1 and Opx_2 have similar contents in MREE and both are HREE-depleted, with absolute concentrations below the detection limits, (Table 1, Fig. 4D). This indicates that both generations of orthopyroxene formed in the presence of garnet. On the other hand, the two orthopyroxene generations show significant differences in LREE concentrations. Opx_1 is LREE-depleted, consistent with an ultramafic orthopyroxene relic, whereas Opx_2 is LREE-enriched (Fig. 4D). Furthermore, Opx_2 has higher Ni content than Opx_1, resembling the Ni concentration of the replaced olivine (Table 1).

4.3. Chemistry of polyphase inclusions

Due to the very fine grain size, the major element concentrations of minerals composing the polyphase inclusions in the Grt_2 core could only be qualitatively determined by scanning electron microscopy (SEM). The opaque phase mainly consists of Al-spinel, or occasionally Fe–Ni-rich sulfides. The remaining 80–90 vol.% of

Table 2
Trace element concentrations (ppm) of representative polyphase inclusions and of inclusions after experimental re-homogenisation

	Polyphase inclusions					Host Grt	Re-homogenised inclusions					Host Grt
Li	1.17	1.36	4.06	8.12	18.4	bdl	3.19	1.54	bdl	2.78	3.50	bdl
Be	0.04	0.05	0.17	0.06	2.20	bdl	2.68	1.39	0.99	2.09	3.33	bdl
P	139	194	88.7	228	95.3	181	926	435	714	356	334	217
K	1162	1263	3873	1633	1961	bdl	1787	1079	1678	1502	1830	bdl
Sc	65.7	81.9	44.2	44.1	44.7	67.9	30.6	46.7	46.5	52.1	54.2	62.8
Ti	15.6	20.9	16.6	18.0	21.7	14.0	86.7	47.1	63.4	72.3	77.5	13.6
V	60.2	67.3	57.9	55.7	58.3	66.0	34.2	46.3	65.6	69.5	56.4	72.9
Rb	2.88	3.03	12.6	4.41	5.42	bdl	3.99	2.07	4.47	3.53	4.31	bdl
Sr	11.1	12.6	152	24.0	11.0	0.08	102	22.6	31.6	21.5	28.3	0.06
Y	39.6	48.2	23.1	20.3	27.9	33.1	18.2	27.6	26.4	20.6	14.5	25.6
Zr	2.45	2.81	1.48	1.67	2.38	2.90	11.4	9.29	12.1	15.2	9.76	2.99
Nb	bdl	bdl	0.01	0.03	0.02	0.01	2.41	0.85	1.93	1.37	2.07	0.03
Cs	0.66	0.66	2.19	1.96	1.54	bdl	0.64	0.38	0.38	0.53	0.59	bdl
Ba	160	183	448	115	160	0.31	291	71.5	68.5	89.7	123	0.15
La	0.05	0.12	0.08	0.23	0.13	0.01	2.71	0.72	1.17	1.15	1.08	0.03
Ce	0.15	0.51	0.12	0.53	0.75	0.03	3.62	1.35	1.83	2.17	1.92	0.02
Pr	0.02	0.11	0.01	0.09	0.17	bdl	0.25	0.22	0.21	0.21	0.19	0.03
Nd	0.19	0.68	0.11	0.64	1.30	0.13	0.68	0.38	0.61	0.79	0.74	0.12
Sm	0.32	0.55	0.22	0.58	1.04	0.34	0.28	0.31	0.40	0.42	0.25	0.32
Eu	0.21	0.39	0.17	0.31	0.51	0.25	0.15	0.20	0.18	0.25	0.19	0.23
Gd	1.52	2.34	1.08	1.57	2.54	1.77	0.96	1.38	1.74	1.64	0.94	1.64
Tb	0.47	0.70	0.32	0.36	0.57	0.56	0.28	0.44	0.44	0.42	0.28	0.48
Dy	5.13	6.78	3.04	3.12	4.59	5.16	2.61	4.22	4.06	3.52	2.52	4.10
Ho	1.49	1.81	0.86	0.73	1.05	1.23	0.66	1.03	0.99	0.79	0.47	0.93
Er	5.59	6.15	2.92	2.29	3.13	3.76	2.28	3.24	3.05	2.18	1.54	2.76
Tm	0.95	0.96	0.51	0.32	0.44	0.54	0.36	0.49	0.47	0.34	0.22	0.41
Yb	7.33	6.74	3.86	2.27	2.90	3.64	6.72	7.54	5.11	2.73	2.15	2.80
Lu	1.18	1.02	0.61	0.33	0.44	0.52	0.38	0.50	0.46	0.31	0.25	0.41
Hf	bdl	0.05	bdl	bdl	0.04	0.05	0.35	0.25	0.34	0.48	0.34	0.05
Ta	bdl	bdl	bdl	bdl	bdl	bdl	0.16	0.13	0.14	0.08	0.13	bdl
Pb	17.3	10.4	11.3	15.2	5.14	0.13	88.6	13.3	46.7	11.9	11.9	0.15
Th	0.04	0.14	0.02	0.31	0.09	0.02	0.27	0.11	0.14	0.11	0.09	bdl
U	bdl	0.05	0.02	0.05	0.04	bdl	0.39	0.17	0.50	0.17	0.65	bdl

Inclusion-free garnet domain compositions are also reported.
bdl = below detection limits.

the inclusions is filled with hydrous minerals. Among these, amphibole is the most abundant; it ranges from pargasite to tschermakite compositions, and is characterised by high K_2O contents (0.12–0.44 wt.%). Amphibole is always associated with Mg-rich chlorite and minor talc + phlogopite. Ba-rich phlogopite (BaO up to 1.5 wt.%) and rare apatite may also be present.

To characterise the trace element composition of the polyphase microinclusions, we performed Laser Ablation analyses on the bulk inclusions. A laser spot size larger than the inclusions site was employed permitting bulk inclusion analyses [41]. The disadvantage of this technique is that each analysis represents a mixture of inclusion and host garnet. In order to see which elements are enriched in the inclusion, the normalised trace element patterns of polyphase inclusions are compared with the pattern of inclusion-free domains of the host garnet (black line in Fig. 5). Representative trace element values are reported in Table 2, and the full spectrum of Primitive Mantle (PM) normalised trace elements is shown in Fig. 5. Overall, the trace elements patterns of the polyphase inclusions show compositional homogeneity. The most striking difference is the strong enrichment in LILE and LREE of the inclusions with respect to the host garnet. Inclusions have absolute concentrations of LILE ≥ 10 times PM, with spikes of Cs, Ba and Pb reaching up to 100–300 time PM, of Li and Sr, and enrichments in LREE. The single analytical values have a relatively large spread (grey area in Fig. 5), likely reflecting the different volume proportion of the inclusions affected by the laser, with respect to the host garnet. In fact, the single inclusion or cluster of inclusions occupy from 5 to 25 vol.% of the laser spot. As a consequence, the absolute trace element concentrations of the polyphase inclusions are significantly higher than the ones reported in Table 2.

5. Experimental re-homogenisation of inclusions

A piston cylinder experiment has been performed with the aim to re-homogenise the primary polyphase inclusions in Grt_2. The starting material consisted of layers of inclusion-rich garnets, separated from the garnet-bearing orthopyroxenite, which were alternated with layers of

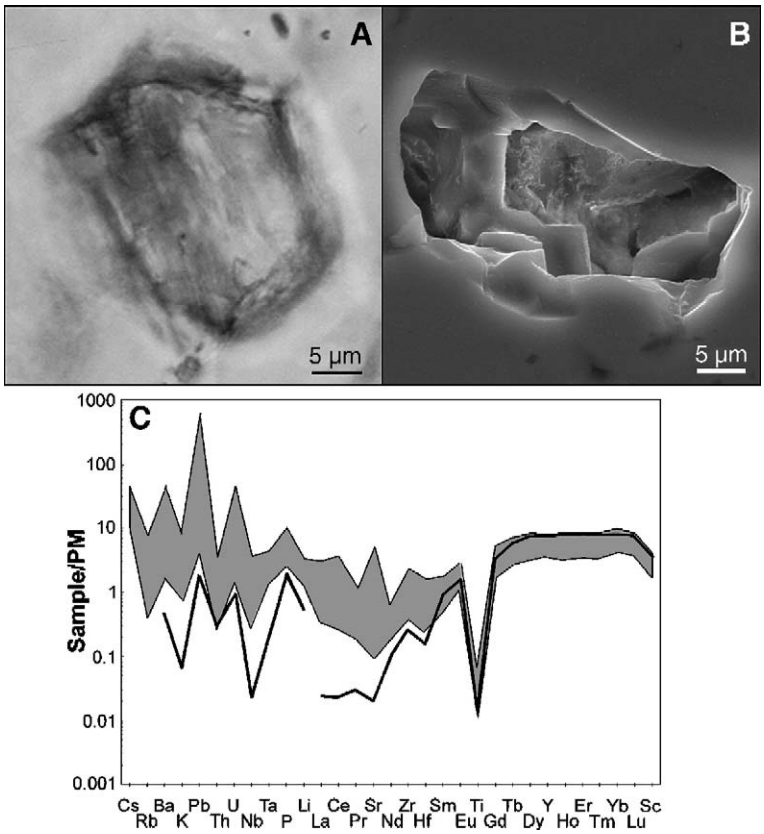

Fig. 6. Photomicrographs of experimentally re-homogenised inclusions. A: Transmitted light image (plane polarised light) of a regularly-shaped single phase inclusion. B: Secondary electron images of inclusion cavities containing porous quench. C: Primitive Mantle [49] normalised trace elements patterns of the analysed re-homogenised inclusions, compared with the average pattern of host garnet analyses.

natural rock powder (see Analytical techniques for detailed explanations). The experiment was run at 3.57 GPa and 900 °C, conditions slightly exceeding the estimated metamorphic peak. The reason for this is twofold. Firstly, the inclusions might have undergone some H_2O loss during retrogression resulting in a higher homogenisation temperature than the one experienced during their formation. Secondly, it places constraints on the position of the wet solidus in the garnet–orthopyroxene-H_2O system which is fundamental to constrain the nature of the fluid phase [12]. After the run, the primary inclusions were all re-homogenised and they appear to be filled by a single isotropic phase (Fig. 6A). Electron microscope images show that the inclusion sites are regularly-shaped cavities, which contain a porous quench residue (Fig. 6B). The orthopyroxenite powder alternated with the garnet layers did not produce any melt in the capsule, indicating that the run conditions were below the wet solidus for a garnet–orthopyroxenite system.

Qualitative major element analyses of the quench material indicate enrichments in Al, Mg and K with respect to the host garnet. Laser Ablation analyses on the re-homogenised inclusions were performed with the same method employed for the former polyphase inclusions. As shown in Table 2 and Fig. 6C, the trace element compositions of the experimentally re-homogenised inclusions are very similar to the calculated compositions of the starting polyphase inclusions. In particular, the PM normalised trace element concentrations again show enrichments in LILE and LREE (Fig. 6C). Moreover, the identical trace element patterns of polyphase and re-homogenised inclusions (c.f. Figs. 5 and 6C), mostly for fluid mobile elements such as the LILE, indicate that no leakage occurred during the experimental re-homogenisation.

6. Discussion

The presented dataset points to the conclusion that the studied garnet–orthopyroxenites derive from garnet–peridotites affected by intense metasomatism during the percolation of a siliceous mobile agent at UHP conditions. Thereafter we will summarise the textural evidence and the compositional features of the analysed orthopyroxenites to discuss the main consequences, in terms of mass transfer and fluid-related processes in a subduction environment.

6.1. Evidence for UHP metasomatism of ultramafic rocks and a model for the formation of garnet–orthopyroxenites

The petrographic observations indicate that the studied orthopyroxenites preserve a relict paragenesis consisting of olivine + Opx_1 + Grt_1 ± clinopyroxene ± Ti-clinohumite overgrown by coarse-grained Opx_2. The latter is associated with porphyroblasts of inclusion-rich Grt_2. Particularly Opx_2 displays evident replacement textures after olivine (Fig. 2A,B) and often includes fine-grained Opx_1. This suggests that former mantle phases (i.e. olivine and Opx_1) were replaced by a Si-enriched phase. Crystallisation of Opx_2 at the expenses of olivine has been described also in oceanic mantle. In such occurrences the replacement of kinked mantle olivine by undeformed orthopyroxene is evidence of the reaction with a silica-saturated liquid which dissolves olivine and precipitates new orthopyroxene [42,43].

The major and trace element compositions of both whole-rock and mineral phases support the textural evidence that the protolith of these pyroxenites was a peridotite. The Mg# and Ni concentrations of the studied samples are high, close to the values of mantle rocks (Fig. 4A). Moreover, their chondrite-normalised REE patterns resemble the ones of a reference Depleted Mantle [39] mostly for MREE and HREE (Fig. 4C). The low CaO contents of the bulk-rocks (0.29–0.36 wt.%) suggest derivation from harzburgites. Concerning the rock-forming minerals, the high Mg# of olivine and orthopyroxene, together with the pyrope-rich composition of garnet (Table 1), are well consistent with the hypothesis that these garnet–orthopyroxenites derive from a mantle peridotite precursor. Moreover, the complementary HREE-enriched and HREE-depleted patterns of garnets (Grt_1 and Grt_2) and pyroxenes (Opx_1, Opx_2 and clinopyroxene) respectively, point to an equilibrium partitioning among these phases (Fig. 4D). Therefore equilibrium growth is interpreted to have occurred in the garnet stability field. The low CaO (0.03–0.09 wt.%) and Al_2O_3 (<0.1 wt.%) in Opx_2 coexisting with clinopyroxene and Grt_2 agree with the *P–T* peak estimates of 4.0 ± 1.0 GPa and 750 ± 50 °C previously reported by Okay [36], Liou and Zhang [31], Zhang et al. [34] and Jahn et al. [35].

With respect to the inferred harzburgite protholith, however, the studied orthopyroxenites show peculiar enrichments in some major and trace elements. They display (i) high SiO_2 contents (up to ~ 54 wt.%); (ii) increasing Al_2O_3 with decreasing CaO (Fig. 4B) and (iii) bulk-rock LREE enrichment, with La up to one order of magnitude higher than in the Depleted Mantle. Zhang et al. [34] and Jahn et al. [35] reported extreme LREE enrichments for most of the Maowu mafic–ultramafic rocks and attributed this feature to a shallow pre-UHP metasomatism by crust-derived LREE-enriched (meteoric) fluids. On the other hand, our dataset and observations indicate that the studied garnet–orthopyroxenites record a

deep (garnet-facies) metasomatism. The replacive Opx_2 and clinopyroxene, when present, are LREE-enriched with respect to the relict Opx_1, with compositions resembling the whole-rock REE patterns (Fig. 4D). Opx_2 is in turn characterised by HREE depletion indicating its equilibrium crystallisation with garnet. The LREE-enriched signature of the garnet–orthopyroxenites was therefore acquired during formation of replacive Opx_2 in the garnet stability field. In summary, we attribute the major and trace element enrichment of the garnet–orthopyroxenites to the infiltration of a metasomatic agent rich in SiO_2, Al_2O_3, and incompatible elements at peak UHP conditions.

The most likely rock types, from which the metasomatic agent was sourced, are the country rock gneisses of the peridotites. Field observations and detailed petrography have shown that the Maowu Ultramafic Complex is hosted by biotite gneiss and orthogneiss which share the same UHP evolution [28,30,31,33,35]. Biotite gneiss contains biotite–muscovite-rich layers and abundant epidote porphyroblasts [30,33]. Orthogneiss develops chlorite scistosity along the boundary with mafic/ultramafic bodies and geochemical and isotopic data demonstrated that they have been affected by intense low grade fluid-assisted alteration [35]. This suggests that the country rocks were likely able to liberate discrete amounts of water during prograde HP/UHP metamorphism. The fluid phase liberated from such gneisses might therefore be constrained by the granite–H_2O phase diagram (Fig. 7).

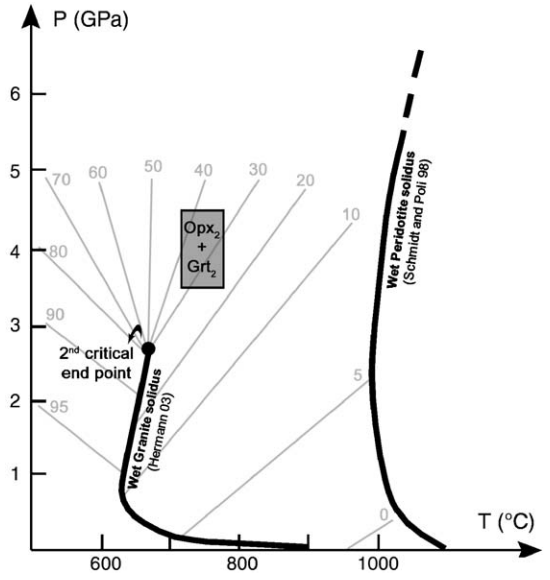

Fig. 7. Estimated peak *P–T* conditions of Maowu ultramafic pyroxenites [31,35,36]. The wet granite solidus [44] and wet peridotite solidus [3] are shown in black solid lines. The grey lines represent the H_2O contents of liquids in a granitic composition as a function of pressure and temperature [44].

A complication arises as the estimated peak metamorphic pressure is likely to be higher than the termination of the wet granite solidus at the second critical endpoint [44]. At peak metamorphic conditions (~ 4.0 Gpa and ~ 750 °C) the composition of the fluid phase is likely a hydrous granitic melt or a very solute rich aqueous fluid (Fig. 7). Such a SiO_2-rich melt-like fluid phase will be highly reactive when in contact with the peridotites. A possible interaction model, which includes all observations, can be summarised by the following generalised reaction:

$$\begin{aligned}&\text{Harzburgite } (Ol + Opx_1 \pm Grt_1 \pm Cpx)\\&\quad + SiO_2 - \text{rich hydrous melt} \rightarrow Grt - \text{orthopyroxenite}\\&\quad \times (Opx_2 + Grt_2) + \text{residual fluid}\end{aligned}$$

This reaction leads to efficient extraction of the major hydrous melt components, Si and Al, by formation of orthopyroxene (Opx_2) and garnet (Grt_2). Such anhydrous phases cannot accommodate the H_2O component of the melt, which evolves into a residual aqueous fluid. The above reaction produces garnet–orthopyroxenites, which are slightly enriched in LREE, due to their partial incorporation in the newly formed Opx_2 (Fig. 4D). However, Opx_2 and Grt_2 are not effective repositories of the incompatible LILE. As will be discussed in the following section, these incompatible elements likely fractionated into the residual aqueous fluid.

6.2. Polyphase inclusions as witnesses of the residual aqueous fluid evolved from the metasomatic SiO_2-rich hydrous melt

There is growing evidence that the polyphase inclusions preserved in peak UHP minerals, such as garnet, can derive from trapped fluids, thus enabling to constrain the nature and composition of the UHP fluid phase. Polyphase inclusions consisting of phlogopite, paragonite, phengite and quartz with minor apatite, rutile and microdiamond, were discovered within garnet of the Erzgebirge diamond-bearing gneisses, Germany [20]. These inclusions have been interpreted as crystallisation products of alkali- and silicate-rich supercritical fluids. Polyphase silicate inclusions in diamond-facies carbonates from the Kokchetav massif (Kazakhstan) have a distinct trace element composition in agreement with the crystallisation from a trapped melt [22]. Microdiamond-bearing polyphase inclusions in garnet–websterite of Western Norway have been related to the entrapment of a percolating UHP fluid phase [21]. At lower metamorphic conditions, such as encountered by the Maowu Complex, it is more difficult to establish the character of the fluid phase. Ferrando et al. [24] investigated polyphase

inclusions in UHP minerals of quartzites and continental eclogites from the Sulu region, which experienced comparable peak pressure and slightly higher temperature (840±50 °C) than the Maowu Complex. The authors proposed that the silicate–carbonate–sulfate inclusions represent supercritical solute-rich aqueous fluids present at peak UHP conditions. The major element composition of the supposed UHP aqueous fluid indicates high amounts of SiO_2, Al_2O_3, SO_4, Na_2O and K_2O in solution. Nevertheless, the major element composition of this fluid, obtained integrating the composition of each inclusion daughter phase, does not resemble the supercritical fluid experimentally determined for the MORB+H_2O system [11,45]. In a recent study Perchuk et al. [25] showed that polyphase hydrous mineral inclusions in UHP garnet could be experimentally homogenised at high pressures and temperatures (4 GPa, 800–1100 °C), indicating that the inclusions derive from a trapped aqueous fluid or hydrous melt. However, this study also shows that such polyphase inclusions likely record retrograde reaction with the host garnet upon cooling.

The polyphase inclusions investigated in this paper are interpreted to have been trapped within coarse UHP garnets during a stage of metasomatic influx of a hydrous granitic melt (Fig. 7). Clusters of irregularly shaped solid inclusions containing microcrystals of clinochlore, enstatite, sapphirine, gedrite, hornblende, talc, phlogopite, corundum, monazite, and rutile have been described in garnets from Maowu orthopyroxenites [31,36]. These inclusions have been interpreted as early phases during garnet growth in a granulite-facies stage pre-dating the Triassic subduction [36]. The inclusions found in our orthopyroxenite samples show textural and compositional differences with respect to the ones described by Okay [36] and Liou and Zhang [31]. They contain a different solid assemblage and display regular negative crystal shapes. The infilling minerals display constant volume ratios, indicating that they represent daughter phases precipitated from a compositionally homogeneous phase (fluid or hydrous melt) primarily trapped by the UHP garnet. The experimental re-homogenisation of the inclusions at P=3.5 GPa and T=900 °C produced a porous quench (Fig. 6A,B), rather than a silicate glass. This demonstrates that the UHP fluid in the inclusions was a solute-rich aqueous solution rather than a hydrous melt. This is confirmed by the fact that no melt was produced in the garnet–orthopyroxene-H_2O system matrix during the experimental run which caused the complete homogenisation of the polyphase solid inclusions. The inclusions thus correspond to a solute-rich aqueous fluid trapped during growth of the host Grt_2. We interprete this fluid as the residual fluid produced with Opx_2 and Grt_2 by the melt-harzburgite reaction. Differently from the reactive hydrous melt, the residual solute-rich fluid is stable with the subsolidus peridotite assemblage at UHP conditions (Fig. 7).

The primary polyphase inclusions contain a number of hydrous phases, such as calcic-K-amphibole, chlorite, talc, Ba-bearing mica, and rare Cl-apatite (Fig. 3), which are indicative of a bulk "mafic" composition of the inclusions. In terms of major elements the inclusions do not reflect the SiO_2-rich agent that firstly metasomatised the system. The similarity of bulk inclusion major elements (determined integrating the composition of each mineral infilling) with the ones of the host garnet suggests a re-equilibration, and probably an interaction, between the trapped fluid and the UHP garnet. The hydrous mineral assemblage filling the inclusions, however, is unstable at peak metamorphic conditions, indicating that recrystallisation of the inclusions occurred during the retrograde decompression of the rocks. These features, particularly the possible exchange between the trapped fluid and the host garnet during such an evolution, prevent a reliable use of the bulk major element composition of the polyphase inclusions determined by the integration of the mineral infillings. On the other hand, the incompatible trace elements did not partition into garnet and remained in the trapped fluid phase. The LA-ICP-MS analysis of the polyphase inclusions thus gives a reliable estimate of the trace element composition of the trapped residual fluid. Because garnet has very low LREE and LILE it is possible to detect even small quantities of these elements within the inclusions. The fact that we were able to re-homogenise the inclusions and the overall consistent trace element patterns of more than 50 analysed inclusions (Fig. 5), indicates that there was no significant loss of fluid and trace elements from the inclusions during decompression. Consequently, the trace element analyses of polyphase inclusions give crucial information about the composition of the fluid present at peak metamorphic conditions.

Both polyphase and re-homogenised inclusions show very high concentrations in incompatible and fluid-mobile trace elements, with spikes in Cs, Ba, Pb, Sr, and a high U–Th ratio (Figs. 5 and 6C, and Table 2). These chemical characteristics provide evidence that the metasomatic agent leading to the formation of the orthopyroxenites had a crustal affinity. The inclusion sites occupied 5 to 25 vol. % of the laser spot during the LA ICP MS analysis. Therefore, the absolute values of trace elements pertaining to the mineral infillings (i.e. LILE and LREE) have been calculated on the basis of garnet/inclusion volume proportions. The dashed black line in Fig. 8 represents the best estimate of inclusion fluid-mobile element concentrations,

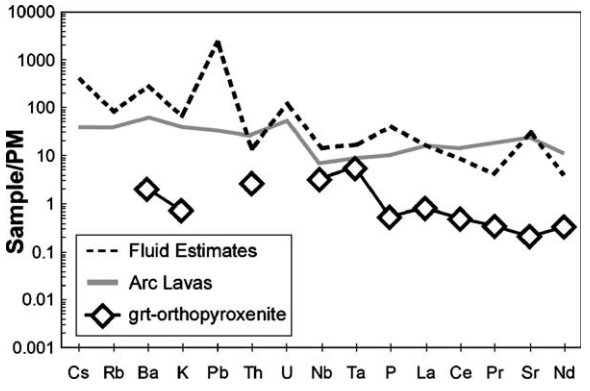

Fig. 8. Primitive Mantle (PM) [49] normalised trace element patterns of the estimated residual fluid concentrations calculated on the basis of garnet/inclusion volume proportions. The most incompatible fluid-mobile elements are compared with the average pattern of Aleutian arc lavas [47] and with the whole-rock orthopyroxenite.

which can reach up to 1000–2000 times PM. The enriched patterns characteristic of the inclusions suggest that the most incompatible elements, derived by the reacting hydrous-melt, prevalently partitioned in the residual fluid. In fact, the whole-rock composition shows enrichments only in LREE (Figs. 4C and 8), whereas most of the fluid-mobile elements are below the detection limits (Table 1). The reason for this observation is that the rock-forming minerals – orthopyroxene and garnet – are not able to incorporate these incompatible elements. The low levels of LILE in the whole-rocks imply that such LILE-enriched fluid largely escaped the system and was only occasionally trapped in Grt_2 to form the polyphase inclusions.

6.3. Implications for trace element transfer in the sub-arc mantle

The case study presented here can be used as proxy to describe the behaviour and compositional evolution of the fluid-mediated slab-to-mantle element transfer at sub-arc depths. Although the studied orthopyroxenites are not direct samples of a mantle wedge, they represent former garnet–peridotites which underwent significant metasomatism driven by the influx of crust-derived SiO_2-rich fluid phases (hydrous melts) at ~ 4.0 GPa and ~ 750 °C, which correspond well to the conditions encountered by the subducted crust at sub-arc depth. The processes occurring in the felsic–ultramafic system studied here are likely representative of interactions taking place between subducted sediments and the overlying mantle. At sub-arc depths the subducted sediments likely undergo partial melting at 750–800 °C [46], producing hydrous silicate melts rich in incompatible elements. According to Manning [10], such crust-derived melts lose the compatible elements, Si and Al, close to their source, i.e. the subducting slab. This is in agreement with the reaction proposed above, which describes the production of garnet–orthopyroxenites at the slab-mantle interface. Mafic crust represents another important trace element reservoir in the subducted oceanic crust. Kessel et al. [11] have recently shown that at $P > 5$ GPa a supercritical fluid phase can be produced in this system. The experimentally produced fluid phase displays silica saturation and is therefore reactive with respect to a Si-undersaturated system, such as the mantle wedge [45]. Therefore, fluid phases extracted from the mafic part of the subducted crust may also potentially react with the mantle wedge peridotites to produce an orthopyroxene-rich reaction zone.

The silicate melts and the supercritical fluids which exit the slabs can therefore be filtered by the overlying mantle to produce a residual aqueous fluid enriched in the most incompatible elements, such as LILE. This fluid is in equilibrium with the peridotite minerals and therefore is able to escape and metasomatise the locus of partial melting in the mantle wedge. To our knowledge, this study provides for the first time direct analysis of the trace element composition of such a fluid. As shown in Fig. 8, the pattern of the residual fluid resembles the trace element pattern of arc lavas, with enrichments in LILE. This trace element signature in arc lavas has been attributed to the addition of a "subduction component" that derives from the subducted sediments [2,47]. This suggests that such a residual fluid is able to transfer the crustal signature from the slab to the mantle wedge, in agreement with the theoretical model described by Manning [10]. An important aspect of such a fluid-mediated trace element transfer is that it occurs at a depth exceeding the stability field of amphibole in peridotites [3]. At pressures below 3.0 GPa, the slab-derived aqueous fluids will react with the mantle wedge minerals and produce amphibole which is enriched in incompatible trace elements, as observed in the Ulten zone peridotites [19]. Such amphibole displays trace element patterns with remarkable similarities to the patterns of the polyphase inclusions (positive spikes in Ba, Pb, Sr and a high U–Th ratio). The trace element transfer in the mantle wedge at pressures below 3.0 GPa is therefore complicated by the stability of amphibole which incorporates significant amounts of incompatible elements. In contrast, at higher pressures the crustal metasomatism of the mantle wedge leads to the formation of garnet–orthopyroxenites that, apart from minor amount of LREE, are not able to retain other incompatible trace elements. Therefore, we expect that

garnet–orthopyroxenite similar to those studied here might form as metasomatised layers at the slab interface acting as filters for fluid/melt-mediated element transfer from the subducted crust to the overlying mantle.

The formation of orhopyroxene-rich layers in the mantle wedge as consequence of sediment melting and/or mafic crust dehydration at sub-arc depths is in agreement with new recent geochemical data on primitive basaltic andesites in North California [48]. The isotopic and geochemical study of andesites from the Mt. Shasta region (USA) indicates that these lavas preserve a remarkable record of subducted lithosphere and mantle wedge elemental contributions. Grove et al. [48] demonstrated that these basaltic andesites could derive from a low degree melt of a garnet + clinopyroxene slab-derived source.

7. Conclusions

Polyphase inclusions trapped in UHP garnets from metasomatically formed garnet–orthopyroxenites are characterised by high LREE contents, a pronounced enrichment in LILE, especially of Cs, Ba, Pb and high U/Th. The inclusions can be experimentally homogenised indicating that they originate from trapped residual aqueous fluids. These trace element-rich fluids most likely form when a crust-derived hydrous granitic melt reacts with harzburgite to form new garnet and orthopyroxene. In contrast to the incoming crustal melt, the residual fluid sampled in the polyphase inclusions is in equilibrium with a mantle mineralogy and, therefore, is able to transfer the crustal trace element signature within the mantle wedge to the locus of fluid-assisted mantle melting.

Acknowledgments

This research was developed by N. Malaspina during her permanence at the Research School of Earth Sciences, ANU, Canberra. The analytical assistance of A. Norris, C. Allen and M. Shelley for laser ablation and electron microprobe at the Research School of Earth Sciences, and the help of L. Negretti for SEM analyses at the University of Genova are greatly acknowledged. Discussion with E. Rampone and G.B Piccardo, and comments by C. Spandler, have been much appreciated. Critical reviews by anonymous reviewers helped to improve the manuscript. N. Malaspina and M. Scambelluri acknowledge funding by the Italian MIUR-Cofin to the project "*C–O–H fluids, hydrates, carbonates and crust–mantle mass transfer in subduction zones*". J. Hermann acknowledges financial support by the Australian Research Council and the Swiss National Science Foundation.

References

[1] Y. Tatsumi, Formation of the volcanic front in subduction zones, Geophys. Res. Lett. 17 (1986) 717–720.
[2] T. Plank, C.H. Langmuir, Tracing trace elements from sediment input to volcanic output at subduction zones, Nature 362 (1993) 739–743.
[3] M.W. Schmidt, S. Poli, Experimentally based water budgets for dehydrating slabs and consequences for arc magma generation, Earth Planet. Sci. Lett. 163 (1998) 361–379.
[4] P.E. van Keken, The structure and dynamics of the mantle wedge, Earth Planet. Sci. Lett. 215 (2003) 323–338.
[5] C.E. Manning, The solubility of quartz in the lower crust and upper mantle, Geochim. Cosmochim. Acta 58 (1994) 4831–4839.
[6] N. Zotov, H. Keppler, In-situ Raman spectra of dissolved silica species in aqueous fluids to 900 °C and 14 kbar, Am. Mineral. 85 (2000) 600–603.
[7] R.C. Newton, C.E. Manning, Solubility of enstatite + forsterite in H_2O at deep crust/upper mantle conditions: 4 to 15 kbar and 700 to 900 °C, Geochim. Cosmochim. Acta 66 (2002) 4165–4176.
[8] H. Bureau, H. Keppler, Complete miscibility between silicate melts and hydrous fluids in the upper mantle: experimental evidence and geochemical implications, Earth Planet. Sci. Lett. 165 (1999) 187–196.
[9] M. Scambelluri, P. Philippot, Deep fluids in subduction zones, Lithos 55 (2001) 213–227.
[10] C.E. Manning, The chemistry of subduction zone fluids, Earth Planet. Sci. Lett. 223 (2004) 1–16.
[11] R. Kessel, M.W. Schmidt, P. Ulmer, T. Pettke, Trace element signature of subduction-zone fluids, melts and supercritical liquids at 120–180 km depth, Nature 437 (2005) 724–727.
[12] J. Hermann, C. Spandler, A. Hack, A. Korsakov, Aqueous fluids and hydrous melts in high-pressure and ultra-high pressure rocks: implications for element transfer in subduction zones, Lithos (in press) (Electronic publication ahead of print).
[13] J. Ayers, Trace element modeling of aqueous fluid–peridotite interaction in the mantle wedge of subduction zones, Contrib. Mineral. Petrol. 132 (1998) 390–404.
[14] Ph. Vidal, C. Dupuy, R. Maury, M. Richard, Mantle metasomatism above subduction zones: trace-element and radiogenic isotope characteristics of peridotite xenoliths from Batan Island (Philippines), Geology 17 (1989) 1115–1118.
[15] R.C. Maury, M.J. Defant, J.L. Joron, Metasomatism of the sub-arc mantle inferred from trace elements in Philippine xenoliths, Nature 360 (1992) 661–663.
[16] A. Laurora, M. Mazzucchelli, G. Rivalenti, R. Vannucci, A. Zanetti, M.A. Barbieri, C.A. Cingolati, Metasomatism and melting in carbonated peridotite xenoliths from the mantle wedge: the Gobernador Gregores case (Southern Patagonia), J. Petrol. 42 (2001) 69–87.
[17] H.K. Brueckner, A sinking intrusion model for the introduction of garnet-bearing peridotites into continent collision orogens, Geology 26 (1998) 631–634.
[18] J.G. Liou, T. Tsujimori, R.Y. Zhang, I. Katayama, S. Maruyama, Global UHP Metamorphism and Continental Subduction/Collision: the Himalayan Model, Int. Geol. Rev. 46 (2004) 1–27.
[19] M. Scambelluri, J. Hermann, L. Morten, E. Rampone, Melt versus fluid induced metasomatism in spinel to garnet wedge peridotites (Ulten Zone, Eastern Italian Alps): clues from trace elements and Li abundances, Contrib. Mineral. Petrol. 151 (2006) 372–394.
[20] B. Stöckhert, J. Duyster, C. Trepmann, H.J. Massonne, Microdiamond daughter crystals precipitated from supercritical COH plus

silicate fluids included in garnet, Erzgebirge, Germany, Geology 29 (2001) 391–394.
[21] H.L.M. van Roermund, D.A. Carswell, M.R. Drury, T.C. Heijboer, Microdiamonds in a megacrystic garnet websterite pod from Bardane on the island of Fjortoft, western Norway: evidence for diamond formation in mantle rocks during deep continental subduction, Geology 30 (2002) 959–962.
[22] A.V. Korsakov, J. Hermann, Silicate and carbonate melt inclusions associated with diamonds in deeply subducted carbonate rocks, Earth Planet. Sci. Lett. 241 (2006) 104–118.
[23] S.L. Hwang, T.F. Yui, H.T. Chu, P. Shen, Submicron polyphase inclusions in garnet from the Tananao Metamorphic Complex, Taiwan: a key to unravelling otherwise unrecognized metamorphic events, J. Metamorph. Geol. 29 (2001) 599–605.
[24] S. Ferrando, M.L. Frezzotti, L. Dallai, R. Compagnoni, Multiphase solid inclusions in UHP rocks (Su-Lu, China): remnants of supercritical silicate-rich aqueous fluids released during continental subduction, Chem. Geol. 223 (2005) 68–81.
[25] A.L. Perchuk, M. Burchard, W.V. Maresch, H.P. Schertl, Fluid-mediated modification of garnet interiors under ultrahigh-pressure conditions, Terra Nova 17 (2005) 545–553.
[26] M. Scambelluri, P. Bottazzi, V. Trommsdorff, R. Vannucci, J. Hermann, M.T. Gòmez-Pugnaire, V. Lòpez-Sànchez Vizcàino, Incompatible element-rich fluids released by antigorite breakdown in deeply subducted mantle, Earth Planet. Sci. Lett. 192 (2001) 457–470.
[27] M. Scambelluri, O. Muentener, L. Ottolini, T. Pettke, R. Vannucci, The fate of B, Cl and Li in the subducted oceanic mantle and in the antigorite-breakdown fluids, Earth Planet. Sci. Lett. 222 (2004) 217–234.
[28] X. Wang, J.G. Liou, Regional ultrahigh-pressure metamorphic terrane in central China: evidence from coesite-bearing eclogite, marble and metapelite, Geology 19 (1991) 933–936.
[29] N.V. Sobolev, V.S. Shatsky, M.A. Vavilov, S.V. Goryainov, Zircon from ultrahigh-pressure metamorphic rocks of folded regions as an unique container of inclusions of diamond, coesite and coexisting minerals, Dokl. Akad. Nauk 334 (1994) 488–492.
[30] F. Xue, D.B. Rowley, J. Baker, Refolded syn-ultrahigh-pressure thrust sheets in the south Dabie complex, China: field evidence and tectonic implications, Geology 5 (1996) 455–458.
[31] J.G. Liou, R.Y. Zhang, Petrogenesis of an ultrahigh-pressure garnet-bearing ultramafic body from Maowu, Dabie Mountains, east-central China, Isl. Arc 7 (1998) 115–134.
[32] J.G. Liou, R.Y. Zhang, E.A. Eide, X.M. Wang, W.G. Ernst, S. Maruyama, Metamorphism and tectonics of high-P and ultra-high-P belts in the Dabie-Su-Lu region, eastern central China, in: A. Yin, M.T. Harrison (Eds.), The tectonic evolution of Asia, Cambridge University Press, 1996, pp. 300–334.
[33] X. Wang, J.G. Liou, S. Maruyama, Coesite-bearing eclogites from the Dabie Mountains, Central China: petrogenesis, P-T paths, and implications for regional tectonics, J. Geol. 100 (1992) 231–250.
[34] R.Y. Zhang, D. Rumble III, J.G. Liou, Q.C. Wang, Low $\delta^{18}O$, ultrahigh-P garnet-bearing mafic and ultramafic rocks from Dabie Shan, China, Chem. Geol. 150 (1998) 161–170.
[35] B. Jahn, Q. Fan, J.J. Yang, O. Henin, Petrogenesis of the Maowu pyroxenite–eclogite from the UHP metamorphic terrane of Dabieshan: chemical and isotopic constraints, Lithos 70 (2003) 243–267.
[36] A.I. Okay, Sapphirine and Ti-clinohumite in ultra-high-pressure garnet–pyroxenite and eclogite from Dabie Shan, China, Contrib. Mineral. Petrol. 116 (1994) 145–155.
[37] N.J.G. Pearce, W.T. Perkins, J.A. Westgate, M.P. Gorton, S.E. Jackson, C.R. Neal, S.P. Chenery, A compilation of new and published major and trace element data for NIST SRM 610 and NIST SRM 612 glass reference materials, Geostand. Newsl. 21 (1997) 115–144.
[38] S.A. Wilson, The collection, preparation, and testing of USGS reference material BCR-2, Columbia River, Basalt, U.S. Geological Survey Open-File Report, vol. 98, 1997.
[39] V. Salters, A. Stracke, Composition of the depleted mantle, Geochem. Geophys. Geosyst. 5 (2004) 1525–2027.
[40] J.-L. Bodinier, M. Godard, Orogenic, ophiolitic, and abyssal peridotites, in: H.D. Holland, K.K. Turrekian (Eds.), Treatise on Geochemistry, Elsevier, Amsterdam, 2004, pp. 103–170.
[41] C.A. Heinrich, T. Pettke, W.E. Halter, M. Aigner-Torres, A. Audétat, D. Günther, B. Hattendorf, D. Bleiner, M. Guillong, I. Horn, Quantitative multi-element analysis of minerals, fluid and melt inclusions by laser-ablation inductively-coupled-plasma mass-spectrometry, Geochim. Cosmochim. Acta 67 (2003) 3473–3497.
[42] G.B. Piccardo, O. Müntener, A. Zanetti, A. Romairone, S. Bruzzone, E. Poggi, G. Spagnolo, The Lanzo South peridotite: melt/peridotite interaction in the mantle lithosphere of the Jurassic Ligurian Tethys, Ofioliti 29 (2004) 37–62.
[43] G. Suhr, E. Hellebrand, J.E. Snow, H.A. Seck, A.W. Hofmann, Significance of large, refractory dunite bodies in the upper mantle of the Bay of Islands Ophiolite, Geochem. Geophys. Geosyst. 4 (2003) 8605, doi:10.1029/2001GC000277.
[44] J. Hermann, Experimental evidence for diamond-facies metamorphism in the Dora-Maira massif, Lithos 70 (2003) 163–182.
[45] R. Kessel, P. Ulmer, T. Pettke, M.W. Schmidt, A.B. Thompson, The water-basalt system at 4 to 6 GPa: phase relations and second critical endpoint in a K-free eclogite at 700 to 1400 °C, Earth Planet. Sci. Lett. 237 (2005) 873–892.
[46] J. Hermann, D.H. Green, Experimental constraints on high pressure melting in subducted crust, Earth Planet. Sci. Lett. 188 (2001) 149–168.
[47] T. Plank, C.H. Langmuir, The chemical composition of subducting sediment: implications for the crust and mantle, Chem. Geol. 145 (1998) 325–394.
[48] T.L. Grove, M.B. Baker, R.C. Price, S.W. Parman, L.T. Elkins-Tanton, N. Chatterjee, O. Müntener, Magnesian andesite and dacite lavas from Mt. Shasta, northern California: products of fractional crystallization of H_2O-rich mantle melts, Contrib. Mineral. Petrol. 148 (2005) 542–565.
[49] K. Bucher, M. Frey, Petrogenesis of metamorphic rocks, Springer-Verlag, Berlin, 1994, 318 pp.
[50] N. Malaspina, J. Hermann, M. Scambelluri, R. Compagnoni, Multistage metasomatism in ultrahigh-pressure mafic rocks from the North Dabie Complex (China), Lithos 90 (2006) 19–42.
[51] W.F. McDonough, S.S. Sun, Composition of the Earth, Chem. Geol. 120 (1995) 223–253.